First-Pass Ventricular Ejection Fraction Using a Single-Crystal Nuclear Camera

Kenneth Nichols, E. Gordon DePuey, Nihal Gooneratne, Helene Salensky, Marvin Friedman and Steven Cochoff

Division of Nuclear Medicine, Department of Radiology; Division of Cardiology, Department of Medicine, St. Luke's-Roosevelt Hospital Center and Columbia University College of Physicians and Surgeons, New York, New York; Christ Hospital and Medical Center, Oak Lawn, Illinois; and General Electric Medical Systems, Milwaukee, Wisconsin

The purpose of the study was to evaluate the reliability of ejection fractions obtained from first-pass radionuclide ventriculography with a large field-of-view tomographic single-crystal gamma camera. **Methods:** A SPECT camera had its electronics redesigned to improve counting efficiency and was equipped with an experimental ultra-high sensitivity collimator. Left ventricular ejection fraction (LVEF) was measured in 28 patients by 30° RAO first-pass imaging and by "best septal view" LAO planar equilibrium radionuclide ventriculography on a conventional small field of view Anger camera. For 28 other patients, first-pass ejection fractions were compared to multicrystal gamma camera values. Visual analysis was performed to judge clinical acceptability of first-pass images for identification of wall-motion abnormalities. **Results:** Linear regression analysis of first-pass against equilibrium ejection fraction demonstrated good correlation ($r = 0.92$; slope = 0.90; intercept = 3.8; s.e.e. = 6.4%). First-pass ejection fraction values also correlated linearly with multicrystal camera values for the left ventricle ($r = 0.94$; slope = 1.05; intercept = 1.3; s.e.e. = 5.3%). For a subgroup of 19 patients, single-crystal camera right ventricle ejection fraction demonstrated good correlation with multicrystal camera values ($r = 0.82$; slope = 1.15; intercept = 1.3; s.e.e. = 6.1%). Interobserver variability correlated as $r = 0.99$ for LVEF ejection fraction and $r = 0.92$ for RVEF. Chi-square analysis of single-crystal first-pass image visual scores versus those from the gated equilibrium acquisitions showed close agreement ($p < 10^{-8}$). **Conclusions:** The evaluated camera/collimator system measured left and right ventricular ejection fraction accurately. Lung frame correction and dual regions were superior to paraventricular background correction and a fixed end-diastolic region.

Key Words: ejection fraction; first pass; single-crystal gamma camera; processing options

J Nucl Med 1994; 35:1292–1300

Early Anger camera count rates were so much lower than multicrystal cameras that counts acquired with single-crystal cameras were inadequate for left ventricular ejection fractions (LVEF), and most first-pass nuclear cardiac imaging was performed with multicrystal cameras (*1–3*). In radionuclide imaging there have always been trade-offs between higher count rates from multicrystal cameras versus better spatial resolution with Anger cameras (*4*). During the 1980s the electronics of small field of view digital Anger cameras were sufficiently improved to obtain accurate first-pass ejection fractions (*5,6*). But during that period camera manufacturers concentrated on improving rotational stability of spatial resolution, energy resolution and flood uniformity characteristics of SPECT cameras rather than on augmenting their count rate capability (*7–9*). In recent years, large field-of-view single-crystal SPECT camera detector electronics have also been enhanced to provide higher count rates (*10*).

With the introduction of ^{99m}Tc labeled myocardial perfusion tracers for which as much as 1.11 GBq (30 mCi) may be injected, it is possible to obtain ventricular function information (*11–17*), which is adjunctive to SPECT myocardial perfusion data in the evaluation of patients with coronary artery disease (*18*). In reports incorporating function and perfusion information, first-pass imaging of ^{99m}Tc-sestamibi was performed with a multicrystal camera (*11–14*), or with a digital Anger camera (*15,16*), but subsequent myocardial perfusion tomograms were acquired using separate large field of view SPECT cameras. However, there may be circumstances under which it is desirable to use just one camera for both first-pass imaging and tomography, especially considering the expense of a two-camera approach.

This investigation was undertaken to determine the feasibility of using a current generation large field of view SPECT camera/collimator system for first-pass cardiac imaging. To further exploit the increased count rate capability afforded by faster electronics of a single-crystal detector ("XC/T", General Electric Medical Systems, Milwaukee, WI), an experimental ultrahigh sensitivity collimator was fashioned for acquisition of first-pass cardiac images. First-pass radionuclide ventriculography obtained on this system was compared to both equilibrium radionuclide ventriculography performed on a standard small field of view

Received Sept. 13, 1993; revision accepted Mar. 31, 1994.

For correspondence and reprints contact: Kenneth Nichols, PhD, Division of Cardiology, St. Luke's-Roosevelt Hospital Center, Amsterdam Ave. at 114th St., New York, NY 10025.

single-crystal gamma camera (General Electric mobile camera), and to first-pass imaging with a first-generation multicrystal camera (Baird System-77, Bedford, MA).

METHODS

Initial Camera Characteristics Evaluation

Two experimental camera/collimator systems were employed for this investigation, one at St. Luke's-Roosevelt Hospital in New York and one at Christ Hospital in Oak Lawn, Illinois. Line-spread functions of the new ultrahigh sensitivity collimator were evaluated from digitized images of a commercially available 1-mm diameter, 40-cm long line source filled with 37 MBq (1 mCi) of ^{99m}Tc in 1 cc of water, placed behind a scattering medium of 10 cm of particle board. Images were acquired with a 20% energy window for 2 million counts as 64^2 matrices at a resolution of 0.4 mm/pixel. Count profiles were summed to incorporate all image counts.

The count rate at which a 20% count loss occurs for this class of detectors has been reported as 170 Kcps for ^{99m}Tc with no scatter using a 20% energy window (*10*). To determine the count rate response of the detector to sources with scatter, 1.11 GBq (30 mCi) of ^{99m}Tc were divided into 10 equal 1-cc samples in bottles. After each bottle's activity was measured with a dose calibrator, count rates registered by the camera were observed as more of the bottles were placed behind a 10-cm thick plastic and water phantom.

System response to large, rapid changes of the input count rate was established for realistic clinical situations by observing changes in counts from a point source at the edge of the field of view during eight patient studies.

Patients

For single-crystal first-pass versus equilibrium comparisons, 28 patients scheduled for routine resting equilibrium tests at St. Luke's-Roosevelt Hospital (Group 1) were studied (67% males; age = 63 ± 12 yr). Group 2 consisted of 28 other patients (36% males; age = 63 ± 16 yr) who had first-pass imaging performed with an identical high-count rate single-crystal camera at Christ Hospital, and were later re-imaged by resting multicrystal first-pass studies (delay time = 30 min). Of the Group 2 patients, first-pass data for 19 (26% males; age = 61 ± 17 yr) were judged suitable for right ventricular (RV) EF analysis based on adequacy of bolus integrity. All patients granted written informed consent.

Single-Crystal First-Pass Data Acquisition

Group 1 patients were injected with a bolus of 740–925 MBq (20–25 mCi) ^{99m}Tc-red blood cells labeled using the modified in vivo method. Boluses were delivered into patients' right antecubital veins via an 18-gauge indwelling intravenous catheter, pushed by a 20–30-cc saline flush. A 30% energy window centered on 140 keV was used. First-pass images were acquired using the ultrahigh sensitivity collimator in the RAO-30° projection as 64 × 64 matrices for 1200 frames over 30 sec, simultaneously with R-wave trigger information. The protocol for Group 2 patients differed from the Group 1 patient protocol only in that a bolus of 814–925 MBq (22–25 mCi) ^{99m}Tc-DTPA was injected instead of labeled red blood cells.

Single-Crystal Equilibrium Data Acquisition

For Group 1 patients, equilibrium imaging was performed with a conventional single-crystal camera and low-energy, general-purpose collimator 5 min after injection with the 740–925 MBq

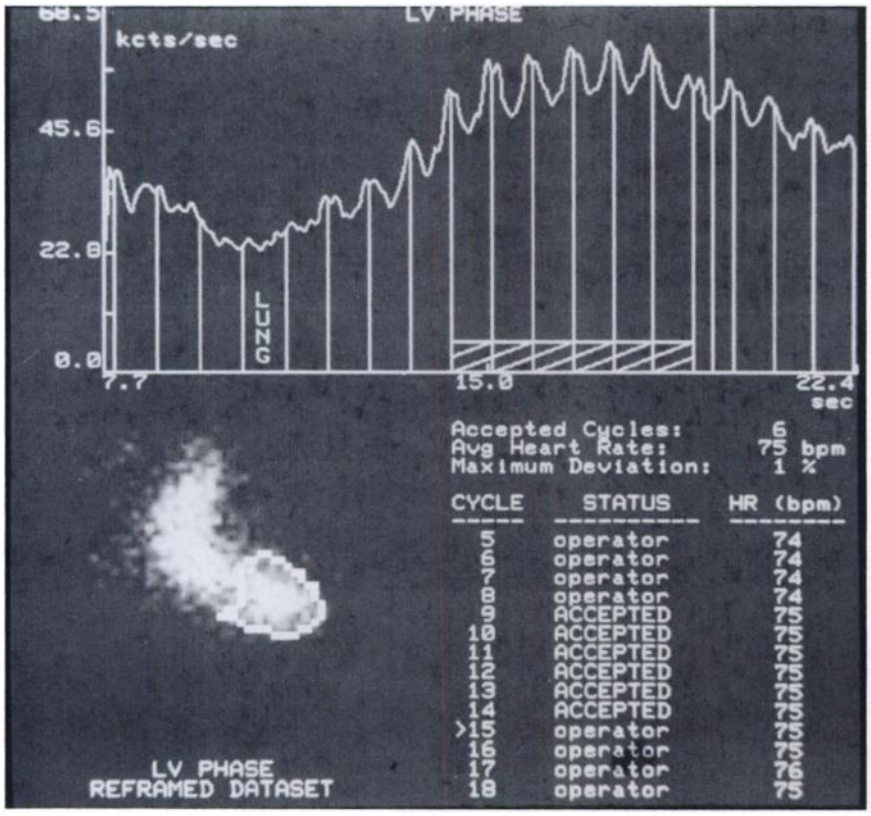

FIGURE 1. Time-activity curve (top) during the left ventricular phase generated from the ROI (lower left) superimposed on image data reframed at 0.5 sec/frame. The R-R intervals which were automatically accepted (lower right) are portrayed on the graph as hatched areas.

(20–25 mCi) of a ^{99m}Tc red blood cell (RBC) bolus. Images were cardiac gated at 32 frames per R-R interval and acquired as anterior, left posterior oblique and left anterior oblique with a caudal tilt angle judged to best separate the LV, left atrium and ventricular septum.

Multicrystal First-Pass Data Acquisition

A first generation multicrystal camera having 14 × 21 NaI(Tl) crystals collimated by a 1.5-inch thick (long bore) multihole lead collimator was used to acquire first-pass data for Group 2 patients. Thirty minutes following single-crystal first-pass ^{99m}Tc-DTPA studies, RAO-30° projection data was acquired of a bolus injection of 740–925 MBq (20–25 mCi) ^{99m}Tc pertechnetate delivered via an indwelling 18-gauge intravenous catheter line followed by a 20-cc saline flush. First-pass images were ungated, acquired as 14 × 21 matrices for 1000 frames at 50 msec per frame.

DATA ANALYSIS AND STATISTICS

Image Processing

Single-crystal camera first-pass images were reframed at 0.1 sec, on which an observer placed a region of interest (ROI) over the superior vena cava to identify beginning and ending times for quality assurance analysis of the bolus shape. The study was discarded if the bolus was fragmented, and transit time was estimated from a gamma variate fit to the first 10 sec of this curve (*19*). Next, the observer identified a frame of the right lung while viewing a composite image of the entire study to draw a region sampling the lung but avoiding the heart. A gamma variate fit to this region's lung curve produced transit time in terms of the number of heart cycles (*20*).

For LV processing, the observer then made an initial estimate of which frames comprised the LV phase of the study by examining a data density curve framed at 0.1 sec while viewing images reframed at 0.5 sec. All images were summed for the selected LV phase time period to form a composite image on which the observer drew an initial estimated LV region. The original 1200-frame dataset was used to construct an initial LV curve including R-wave triggers, and was analyzed automatically for probable acceptable heart beats, excluding those outside ±10% of the average R-R interval (Fig. 1). The observer examined the automatically accepted R-R intervals, modified their selection if necessary, and chose a "lung" frame from those following the RV phase and prior to the LV phase. A filtered representative cycle of 12 frames per R-R interval for the time segments corresponding to accepted representative heart beats within the LV phase was generated from the complete 1200 frame dataset. Guided by the end-diastolic, end-systolic, phase and amplitude images, the observer next refined the LV region as seen on the representative cycle images. EF was computed using the newly refined end-diastolic and end-systolic ROIs superimposed on data of the original data set (Fig. 2).

For LV processing, two background correction methods were evaluated at the beginning of this investigation. Correction for background counts was performed by either subtracting counts of a para-ventricular region defined by the operator, or by a "lung method" (*6,21*) of removing counts to varying degrees throughout the LV phase of the

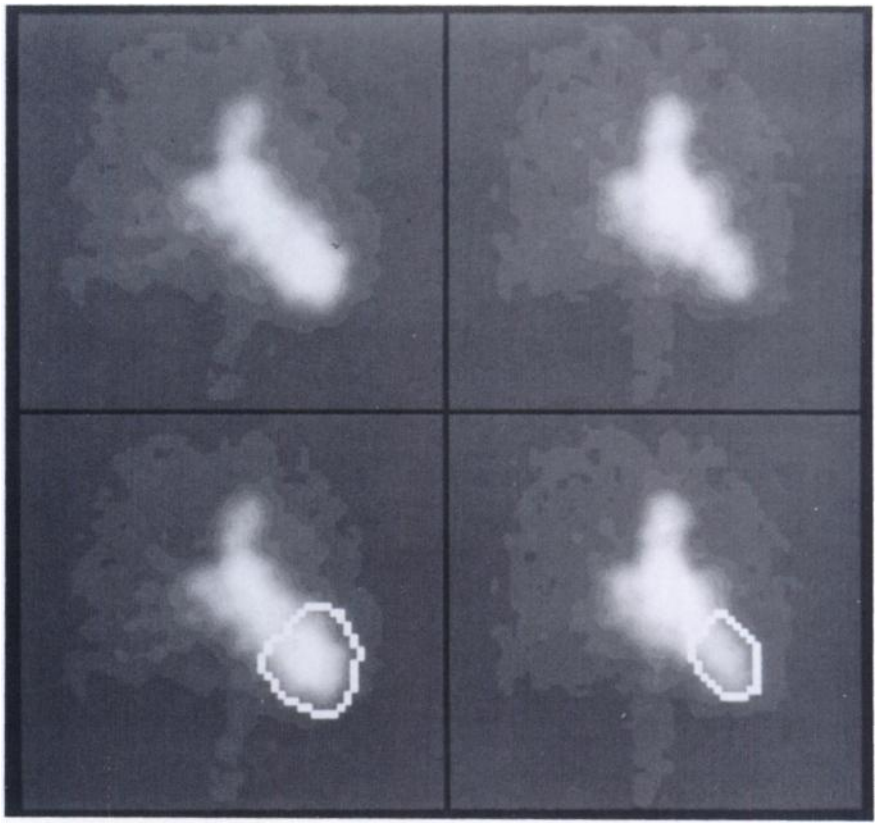

FIGURE 2. End-diastolic (left) and end-systolic (right) frames along with ROIs (bottom) used to compute LVEF for a normal patient (LVEF = 56%).

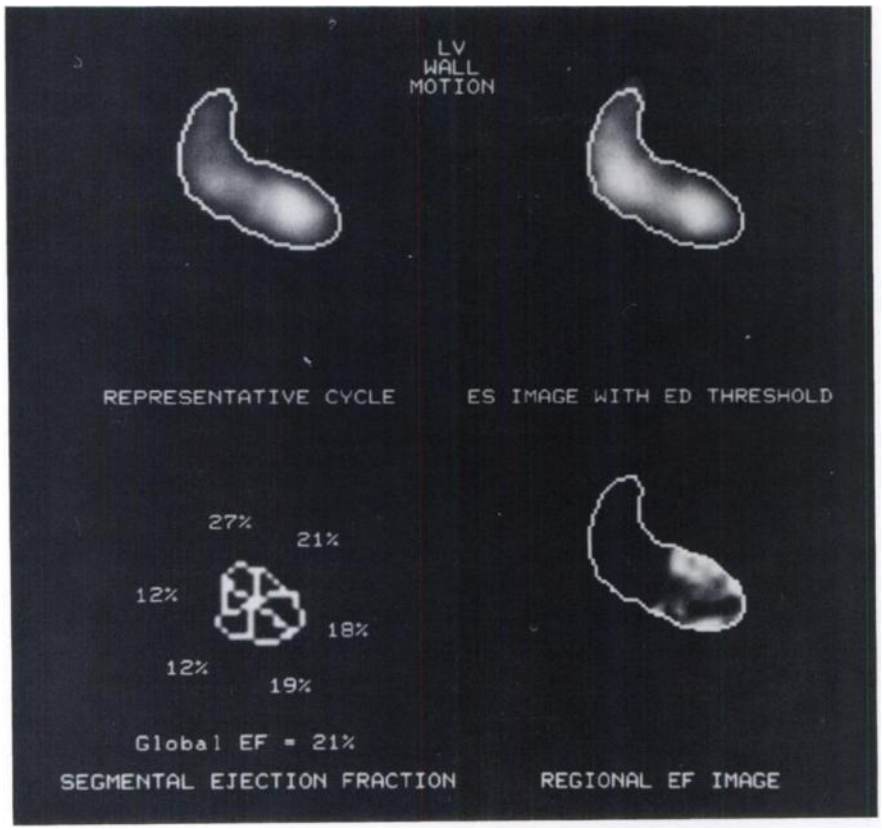

FIGURE 3. An example of an abnormal patient study (LVEF = 27%) demonstrating wall motion abnormalities. End-diastole and end-systole are shown in the upper left and upper right, respectively. The location of segments along with corresponding segmental wall motion values appear in the lower left. The lower left image portrays relative count differences between end-diastole and end-systole.

study based on the observance of lung counts. For each background method, data were further analyzed as to whether LV counts were taken from a single end-diastolic region, or from separately defined end-diastolic and end-systolic regions.

Right-ventricle data analysis proceeded identically to that for the LV up to the point of chamber phase selection, for which RV phase times were estimated from the data density curve by the observer while viewing 0.5-sec images. Data during those times were summed into a single image on which the observer outlined an estimated RV region. Automatic analysis of the original data then identified heartbeats falling within 10% of the average during the RV phase. No form of background correction was applied to RV images. A Hanning filter (cutoff = 0.5) was used on the original 1200-frame gated data to generate a 12-frame image set representative of heartbeats adhering to the predefined R-R limits during the RV phase of bolus transit. Finally, the observer modified the region defining the RV as necessary while observing RV end-diastolic, end-systolic, phase and amplitude images to aid in the separation of the atrium from the ventricle and for outflow tract definition. The original dataset was used to compute RVEF from the final end-diastolic ROI.

Multicrystal first-pass data were processed using standardized methods associated with first-generation multicrystal gamma cameras (Baird System-77 Software Version 10) (*22*), relying on the analysis of the curve of the first pass of the bolus resolved at a sampling time of 50 msec (*23*). The multicrystal camera/computer system's software for residual activity correcting was used to compensate the ^{99m}Tc-pertechnetate injection for the previous ^{99m}Tc-DTPA injection.

Wall Motion Evaluation

A consensus of experienced observers quantified their impressions of wall motion by using a 5-point scale (3 = normal, 2 = mild hypokinesis, 1 = marked hypokinesis, 0 = akinesis, −1 = dyskinesis). They viewed the cinematic playback of the representative cycle of first-pass RAO-30° filtered images, from which motion of inferior, apical and anterior myocardial walls were assessed. On a separate occasion, the observers viewed filtered cinematic playbacks of "best septal view" LAO, anterior and left lateral or LAO-70° equilibrium views displayed simultaneously, and used the same subjective scale to quantify their impressions of the same myocardial regions. The septal and lateral walls, though assessed in the equilibrium views, could not be evaluated from the RAO-30° first-pass images (Fig. 3).

Statistics

Patient population information is indicated in the text as mean ±1 s.d. Linear regression analysis was used to compare EFs from the different methods, and to assess intraobserver and interobserver variability. Evaluation of agreement between wall motion scores was performed by Spearman rank-correlation and chi-square analysis of con-

tingency tables in which scores were paired for each territory.

RESULTS

Collimator Characteristics

While the FWHM of the new ultrahigh sensitivity collimator line-spread function is 21 mm at 10 cm in scatter for ^{99m}Tc (Fig. 4), and therefore on the order of 2 times that of the 10 mm FWHM of the low-energy, general-purpose collimator typical of those routinely employed for nuclear cardiac scanning, it is only 60% of the estimated 37 mm FWHM of the multihole collimators used with first-generation multicrystal cameras employed successfully throughout the 1980s (*2*). The degradation of spatial resolution of the ultrahigh sensitivity collimator is accompanied by increased collimator sensitivity of 4.7 times, compared to the general-purpose collimator, whereas the conventional high-sensitivity collimator is 2.3 times more sensitive than a general-purpose collimator.

Detector Counting Characteristics

For the large field-of-view, single-crystal detector, the count rate at which 20% loss occurred was 140 Kcps for ^{99m}Tc with 10 cm of water scatter (Fig. 5), implying a deadtime of $1.6 \cdot 10^{-6}$ sec (*24*). An extrapolation of the Figure 5 curve to a 100% count loss suggests a maximum count rate of 350 Kcps, although maximum count rates of 600 Kcps have been reported for this detector class (*10*). These values may be compared to maximum count rates of 65 Kcps for the conventional single-crystal camera used in this study for gated equilibrium acquisitions, 250 Kcps for the first-generation multicrystal camera used in this study and 1 Mcps for newer generation multicrystal cameras (*4*).

For the eight-patient data acquisitions performed with a point source in the field of view, point source time-activity curves were generated and corrected for background

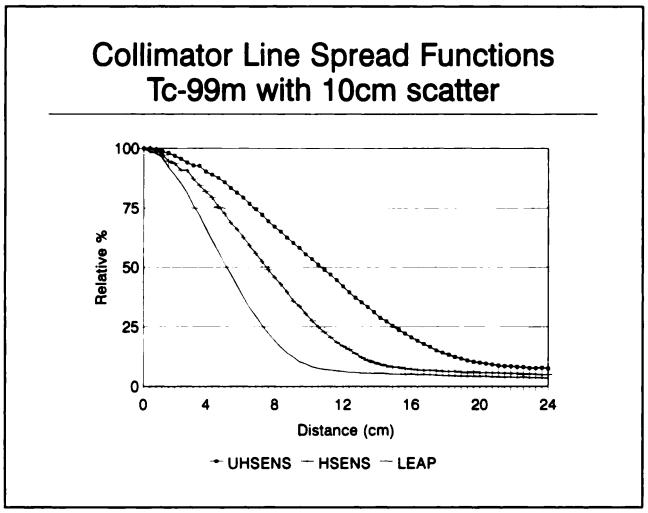

FIGURE 4. Measured line spread functions for ^{99m}Tc in 10-cm plexiglass scatter versus source location for the low-energy, general-purpose (LEGP), high-sensitivity (HSENS) and ultrahigh sensitivity (UHSENS) collimators.

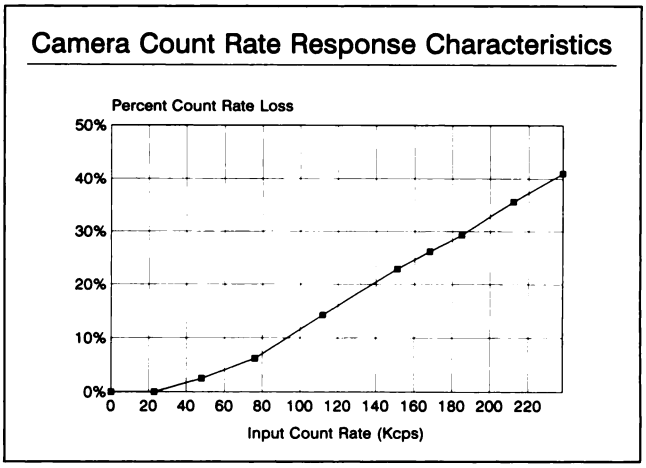

FIGURE 5. Percent count rate loss versus input count rate measured for ^{99m}Tc in 10 cm of water scatter using a 20% energy window without collimators.

counts from neighboring regions. The count rate during the LV phase of first-pass studies averaged 122 ± 20 Kcps (maximum = 179 ± 33 Kcps). Counting efficiency of the camera was 71% ± 8% throughout the LV phase, which lasted 4.3 ± 1.5 sec.

For Group 1 patients, end-diastolic background-corrected counts were 5.0 ± 2.9 Kcounts for the single-crystal, first-pass images and 20.9 ± 11.0 Kcounts for the single-crystal equilibrium images. For Group 2 patients, end-diastolic background-corrected counts were 4.6 ± 2.1 Kcounts for the single-crystal, first-pass images and 6.2 ± 3.5 Kcounts for the multicrystal first-pass images. Thus, for clinical first-pass studies the single-crystal method provided a LV end-diastolic count density approximately 74% of that obtained with the first-generation multicrystal camera.

Ejection Fractions

The results of examining data processing options for the first 20 patients studied are graphed in Figure 6. These methods consisted of the combinations of:

1. para-ventricular region background correction with fixed end-diastolic outline only
2. para-ventricular region background correction with separate end-diastolic and end-systolic outlines
3. "lung frame" background correction with fixed end-diastolic outline only
4. "lung frame" background correction with separate end-diastolic and end-systolic outlines.

Linear correlation coefficients of the single-crystal, first-pass LVEF measurements performed with these four processing methods compared to equilibrium LVEF values were 0.86, 0.91, 0.91 and 0.96, respectively. Based on the highest value of r = 0.96, the lung method background correction together with using separate end-diastolic and end-systolic regions was used for processing all subsequent single-crystal, first-pass LVEF acquisitions and for reprocessing of the initial 20 patient studies.

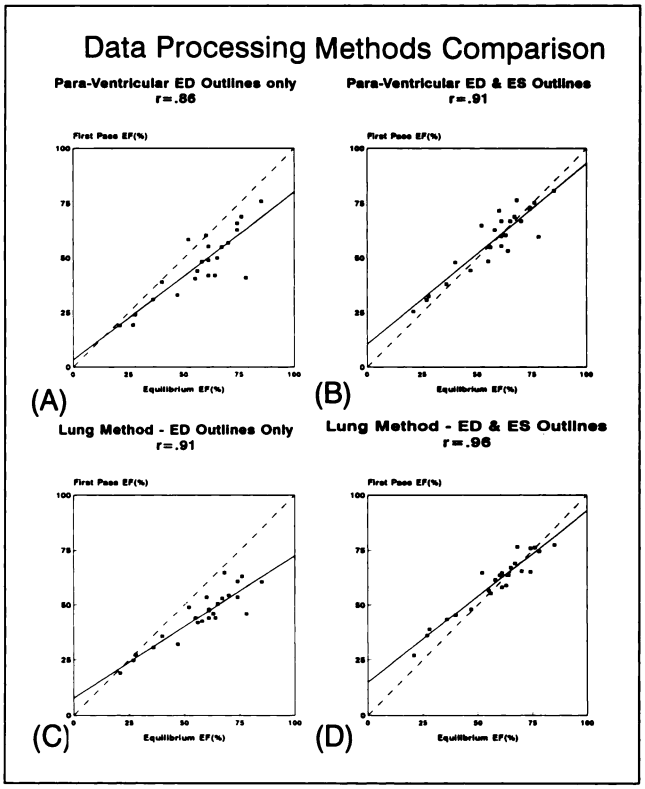

FIGURE 6. Single-crystal (SC) first-pass (FP) LVEF measurements using four data processing methods compared to SC equilibrium (EQ) values in an initial group of 20 patients. Dashed lines = unity and solid lines = least-squares fit.

For Group 1 patients, the number of heart cycles used for the representative heart cycle was 4.7 ± 1.3 beats. Bolus transit averaged 1.6 ± 0.9 sec (*19*), and lung transit was 7.0 ± 2.2 heart beats (*20*). A high degree of linear correlation was found between single-crystal, first-pass LVEF values and equilibrium LVEF measurements (r = 0.92) for Group 1 patients, as well as between the single-crystal, first-pass LVEF and multicrystal first-pass LVEF values for Group 2 patients (r = 0.94) (Fig. 7, Table 1). Excellent intraobserver variability (r = 0.98) and interobserver variability (r = 0.99) correlations of single-crystal, first-pass LVEF measurements were found (Fig. 8, Table 1). No trends were discerned in evaluating measurement differences versus measurement averages of either intraobserver repeatability (r = 0.08), or interobserver agreement (r = 0.19) (Fig. 8).

Linear regression analysis of single-crystal, first-pass RVEF with multicrystal first-pass RVEF values are shown in Figure 9 and Table 2. Individual observer's correlation coefficients ranged from r = 0.69 to r = 0.82 for single-crystal, first-pass RVEF compared to multicrystal first-pass RVEFs. Interobserver variability of single-crystal, first-pass RVEF was r = 0.92 (Table 2, Fig. 10). While there was a significant average difference between the two observers (mean difference = 13.7), no trend was seen in differences versus averages (r = 0.14) (Fig. 10).

Wall Motion Assessment

The number of territories rated at each visual wall motion score for first-pass and equilibrium images are presented in Table 3. For these data, the chi-square was 100.03 for 12 degrees of freedom ($p < 10^{-8}$). Seventy-four territories were judged, for which the Spearman rank correlation test yielded $r_S = 0.915$ ($p = 0.000$).

DISCUSSION

Our study has shown that LVEF values computed from data acquired with the large field of view camera/collimator combination correlate well with established methods and that data processing is highly reproducible. Previous investigators reported correlations between first-generation multicrystal camera first-pass LVEFs compared to small field of view digital single-crystal equilibrium LVEF values ranging from r = 0.83 in 135 patients (*1*) to r = 0.94 in 26 patients (*3*) and r = 0.94 in 64 patients (*25*), consistent with the r = 0.94 correlation we found between multicrystal and large field of view single-crystal camera first-pass LVEFs. Likewise, the r = 0.92 correlation we found between large field of view, single-crystal camera first-pass LVEF values compared to equilibrium values agrees with others' studies comparing first-pass LVEFs to equilibrium LVEFs on the same small field of view, single-crystal digital camera, for which results were r = 0.89 for 19 patients (*26*), and r = 0.91 (*27*) for a group of 17 patients for whom end-diastolic counts exceeded 2000 counts. Previously reported first-pass LVEF interobserver variability linear correlation coefficients ranged from r = 0.77 (*1*) to r = 0.98 (*21*), the latter being consistent with our r = 0.99 result.

Knowledge of RVEF is helpful in some classes of suspected cardiac disease (*28*), although measurement of RVEF by first-pass radionuclide ventriculography is more problematic, primarily due to right atrial overlap, as reflected in the literature for studies reporting little correlation between multicrystal first-pass RVEF compared to single-crystal equilibrium RVEF (r = 0.28) and poor inter-

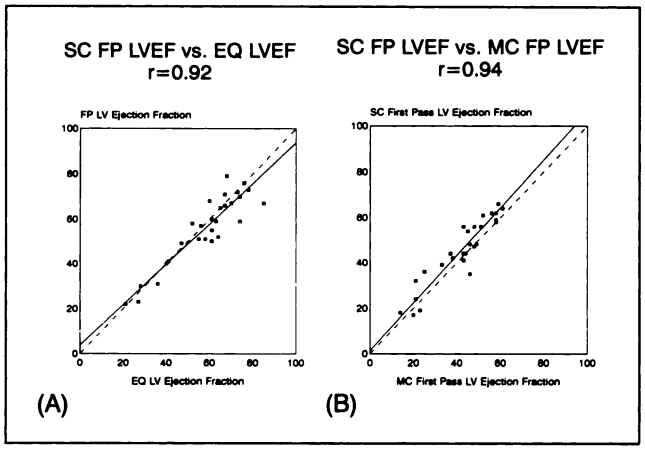

FIGURE 7. (A) Single-crystal (SC) first-pass (FP) LVEF measurements versus EQ values. (B) SCFP LVEF values versus multicrystal (MC) FP LVEF measurements.

TABLE 1
LVEF Data Processing Statistical Comparisons

	Observer 1 SCFP LVEF vs. SCEQ LVEF	Observer 1 SCFP LVEF vs. MCFP LVEF	Observer 1A SCFP LVEF vs. observer 1B SCFP LVEF	Observer 1 SCFP LVEF vs. observer 2 SCFP LVEF
No.	28	28	28	16
r	0.92	0.94	0.98	0.99
Slope	0.90	1.05	0.99	1.02
Intercept	3.8	1.3	0.70	−1.00
s.e.e.	6.4	5.3	3.60	2.90

SCFP = single-crystal, first-pass; SCEQ = single-crystal equilibrium; and MCFP = multicrystal first-pass.

observer variability (r = 0.42) for multicrystal first-pass RVEFs (*1*). More recent studies (*3*) found somewhat better correlation (r = 0.78) between first-pass and equilibrium RVEF from a small field of view gamma camera in 15 patients, and good agreement (*29*) (r = 0.96) between small field of view, single-crystal camera gated first-pass RVEF compared to ultrafast computerized tomography, but weaker correlation between equilibrium RVEF and cine computerized tomography (r = 0.71) and between ungated first-pass curve measurements and cine computerized tomography (r = 0.63) (*29*).

Our correlation of a large field of view, single-crystal camera first-pass RVEF compared to multicrystal RVEF ranged from r = 0.69 to r = 0.82 and our interobserver variability was r = 0.92. We did not attempt to compare first-pass RVEF with equilibrium values due to difficulties with the equilibrium technique for the right heart, as already noted (*1*). Therefore, whereas agreement of RVEFs with the multicrystal camera values is less striking, we attribute this to the relatively greater difficulty of accessing a proven gold standard rather than with inherent limitations of the equipment we investigated. The relatively poorer interobserver variability which we observed for

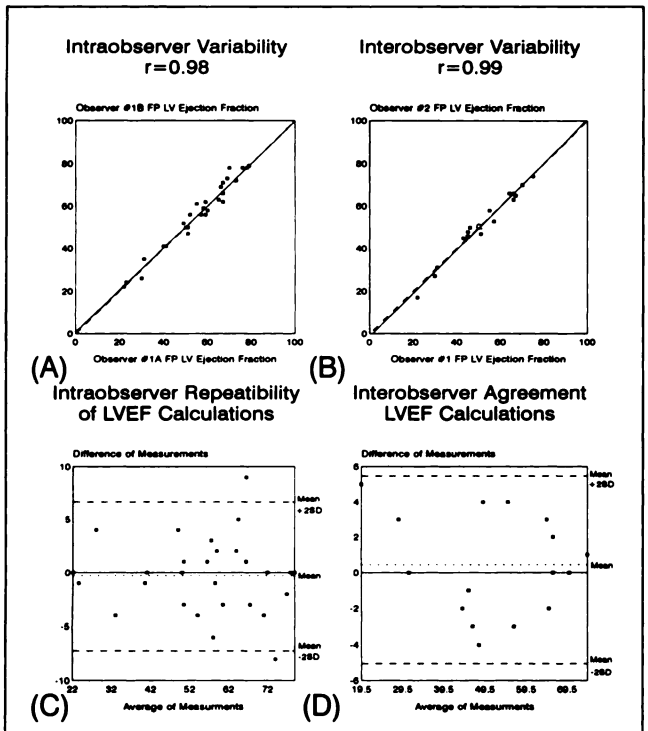

FIGURE 8. (A) Single-crystal (SC), first-pass (FP) LVEF values assessed by an observer on one occasion versus SCFP LVEF measurements on the same patient group by the same observer on a different occasion. (B) SCFP LVEF measurements made by an observer versus SCFP LVEF measurements of the same data by another independent observer. Differences between values are plotted versus averages of values to generate (C) intraobserver repeatability and (D) interobserver agreement.

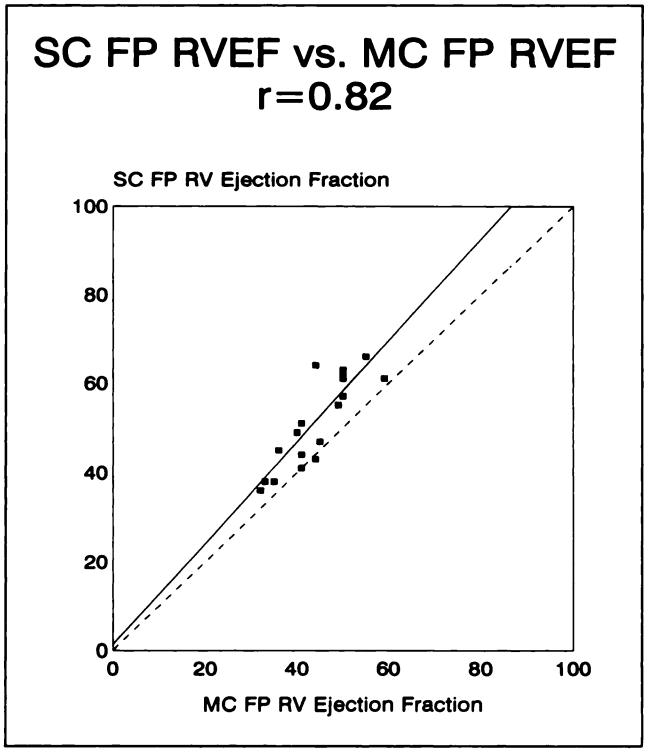

FIGURE 9. Single-crystal (SC) first-pass (FP) RVEF versus multicrystal (MC) FP RVEFs in 19 patients.

TABLE 2
RVEF Data Processing Statistical Comparisons

	Observer 1 SCFP RVEF vs. MCFP RVEF	Observer 2 SCFP RVEF vs. MCFP RVEF	Observer 1 SCFP RVEF vs. Observer 2 SCFP RVEF
No.	19	19	19
r	0.82	0.69	0.92
Slope	1.14	0.83	0.79
Intercept	1.2	14.9	10.3
s.e.e.	6.1	6.60	3.50

SCFP = single-crystal first-pass and MCFP = multicrystal first-pass.

TABLE 3
Contingency Table of First-Pass Visual Wall Motion Scores Against Equilibrium Visual Wall Motion Scores

		Visual First-Pass Wall Motion Scores				
		3	2	1	0	−1
Visual	(3)	42	6	1	0	0
Equilibrium	(2)	0	4	2	0	0
Wall	(1)	0	0	8	1	0
Motion	(0)	0	0	3	5	0
Scores	(−1)	0	0	2	0	0

RVEF calculations was most likely due to difficulty in defining pulmonary and tricuspid valve planes, as others have noted (*30*).

It was demonstrated in the 1970s that first-generation multicrystal camera count rates were adequate for first-pass imaging (*31*). Our investigation has found that count rates with the experimental single-crystal camera/collimator system were roughly comparable (74%) to those of a first-generation multicrystal camera, and well above the 2000-count, end-diastolic LV minimum found to be required for accurate LVEF measurements (*27*), while spatial resolution is 60% better than for a first-generation multicrystal camera.

Image quality was judged to be adequate for visual assessment of wall motion, as demonstrated by the high degree of correlation found between wall motion scores of equilibrium and single-crystal, first-pass images ($p < 10^{-8}$). Consequently, this device provides high quality LV images from first-pass studies as well as accurate LVEF measurements.

First-pass data acquisition does have its pitfalls, however. Patient motion, particularly during exercise testing, is problematic and requires the use of special motion-correction algorithms (*32*). Also, as only a few heartbeats are used to form representative cardiac cycles, some patients with severe arrhythmias may not be suitable for first-pass studies (*33*). Pulmonary hypertension can cause unduly long lung transit times (*33*) with subsequent oversubtraction of background counts, and the uniformity of mixing necessary for accurate EF calculations may not always be achieved (*30*).

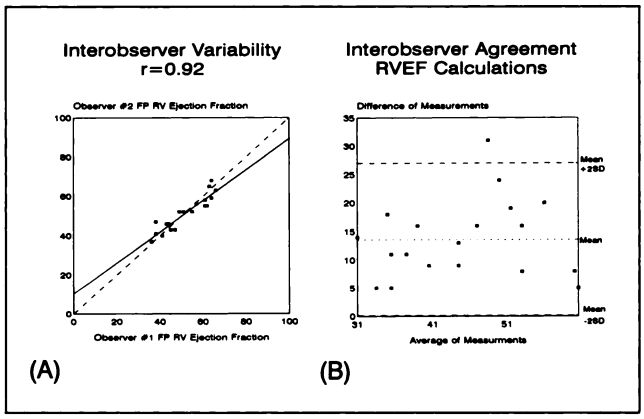

FIGURE 10. (A) Single-crystal (SC) first-pass (FP) RVEF measurements by an observer versus RVEF measurements from the same patient group by another independent observer. (B) Differences of RVEF determinations between the two observers versus averages of values are plotted.

The type of machinery studied in this paper, a large field of view SPECT camera with its fixed horizontal imaging table, is less convenient than a small field of view machine for first-pass imaging in performing peak exercise studies. Also, the camera we studied needs a special ultrahigh sensitivity collimator for first-pass imaging, different from the high-resolution collimator typically used for gated sestamibi SPECT studies, and hence requires changing collimators between function and perfusion studies. It is doubtful that a more standard collimator would have provided adequate counts, considering that we observed average end-diastolic counts of 5.0 ± 2.9 Kcounts using the ultrahigh sensitivity collimator. Given the relative collimator efficiencies described above, a LEAP collimator would have provided only 2.2 Kcounts and high-resolution collimation only 1.1 Kcounts on average, far below the minimum 2 Kcounts per end-diastolic image other investigators have found to be essential for adequate counts (*27*). With too few counts, the delineation of end-diastolic and end-systolic regions becomes too uncertain. This situation can be influenced by the matrix size used to digitize the images, but since we had only 64 × 64 matrices available, we did not explore the possibilities of using coarser matrices, as other investigators have done (*6*).

In conclusion, we have demonstrated that the large field-of-view camera, which is widely used for tomography, can provide adequate first-pass studies. Current generation multicrystal cameras have greatly improved spatial resolution and higher count rate capability than the previous multicrystal camera generation (*4*), exceeding maximum count rates of 1M cps. However, using one of those devices in addition to a separate camera for perfusion tomography is not practical in all institutions. It is anticipated that the additional wall motion and LVEF information obtained from a first-pass study in conjunction with ^{99m}Tc-sestamibi

perfusion tomography will be valuable in forming the overall diagnosis when studying cardiac artery disease in individual patients (*11*). Unlike previous methods which employed rarely used isotopes for the first-pass study (*34–35*) different from those used for perfusion studies, protocols which extract this combined function and perfusion information from a single injection of one isotope are likely to become widely used standards.

ACKNOWLEDGMENTS

The authors thank Chris Smith and Steven Melancon of St. Luke's-Roosevelt Hospital and Gary Smith of Christ Hospital for their assistance in the acquisition of clinical information. This work was supported by a grant from General Electric Medical Systems, Inc.

REFERENCES

1. Kaul S, Boucher CA, Okada RD, Newell JB, Strauss HW, Pohost GM. Sources of variability in the radionuclide angiographic assessment of ejection fraction: a comparison of first-pass and gated equilibrium techniques. *Am J Cardiol* 1984;53:823–828.
2. Wackers FJT. First-pass radionuclide angiography. In: Gerson MC, ed. *Cardiac nuclear medicine*. New York: McGraw-Hill; 1987: 53–66.
3. Bisi G, Sciagra R, Bull U, et al. Assessment of ventricular function with first-pass radionuclide angiography using technetium-99m hexakis-2-methoxyisobutylisonitrile: a European multicentre study. *Eur J Nucl Med* 1991; 18:178–183.
4. DePuey EG, Berger HJ. Evaluation of cardiac function using first pass radionuclide angiocardiography. In: Adam WE, ed. *Handbook of nuclear medicine*, volume 2. New York: Gustav Fisher Verlag;1993:103–126.
5. Mena I, Narahar K, Maublant JC, Brizendine M, Criley M. Simultaneous maximal exercise radionuclide angiography and thallium-201 stress perfusion imaging. *Am J Cardiol* 1984;53:812–817.
6. Gal R, Grenier RP, Carpenter J, Schmidt DH, Port SC. High count rate first-pass radionuclide angiography using a digital gamma camera. *J Nucl Med* 1986;27:198–206.
7. Axelsson B, Israelsson A, Larsson S. Nonuniformity induced artifacts in single-photon emission computed tomography. *Acta Radiol Oncol* 1983;22: 215–224.
8. Jahangir SM, Brill AB, Bizais YJC, et al. Count-rate variations with orientation of gamma detector. *J Nucl Med* 1983;24:356–359.
9. Rogers WL, Clinthorne NH, Harkness BA, Koral KF, Keyes JW. Field-flood requirements for emission computed tomography with an Anger camera. *J Nucl Med* 1982;23:162–168.
10. Lewellen TK, Bice AN, Pollard KR, Zhu J, Plunkett ME. Evaluation of a clinical scintillation camera with pulse tail extrapolation electronics. *J Nucl Med* 1989;30:1554–1558.
11. Berman DS, Kiat H, Maddahi J. The new ^{99m}Tc myocardial perfusion imaging agents: ^{99m}Tc-sestamibi and ^{99m}Tc-teboroxime. *Circulation* 1991; 84(suppl):I7–I21.
12. Iskandrian AS, Heo J, Kong B, Lyons E, Marsch S. Use of technetium-99m isonitrile (RP-30A) in assessing left ventricular perfusion and function at rest and during exercise in coronary artery disease, and comparison with coronary arteriography and exercise thallium-201 SPECT imaging. *Am J Cardiol* 1989;64:270–275.
13. Jones RH, Borges-Neto S, Potts JM. Simultaneous measurement of myocardial perfusion and ventricular function during exercise from a single injection of technetium-99m-sestamibi in coronary artery disease. *Am J Cardiol* 1990;66:68E–71E.
14. Borges-Neto S, Coleman E, Potts JM, Jones RH. Combined exercise radionuclide angiography and single photon emission computed tomography perfusion studies for assessment of coronary artery disease. *Semin Nucl Med* 1991;21:223–229.
15. Baillet G, Mena IG, Kuperas JH, Robertson JM, French WJ. Simultaneous technetium-99m-MIBI angiography and myocardial perfusion imaging. *J Nucl Med* 1989;30:38–44.
16. Villanueva-Meyer J, Mena I, Narahar KA. Simultaneous assessment of left ventricular wall motion and myocardial perfusion with technetium-99m-methoxy isobutyl isonitrile at stress and rest in patients with angina: comparison with thallium-201 SPECT. *J Nucl Med* 1990;31:457–463.
17. Boucher CA, Wackers FJ, Zaret BL, Mena I. Technetium-99m-sestamibi myocardial imaging at rest for assessment of myocardial infarction and first-pass ejection fraction. *Am J Cardiol* 1992;69:22–27.
18. Osbakken MD, Okada RD, Boucher CA, Strauss HW, Pohost GM. Comparison of exercise perfusion and ventricular function imaging: an analysis of factors affecting the diagnostic accuracy of each technique. *J Am Coll Cardiol* 1984;3:272–283.
19. Rozanski A, Rodrigues E, Nichols K, Berman DS. Equilibrium and first-pass radionuclide cineangiography. In: Pohost GM, O'Rourke RA, eds. *Principles and practice of cardiovascular imaging*. Boston: Little, Brown and Company; 1991:221–260.
20. Chu RYL, Peterson RE. Mean pulmonary transit time in first-pass studies. *J Nucl Med Technol* 1988;16:179–182.
21. Gal R, Grenier RP, Schmidt DH, Port SC. Background correction in first-pass radionuclide angiography: comparison of several approaches. *J Nucl Med* 1986;27:1480–1486.
22. Marshall RC, Berger HJ, Costin JC, et al. Assessment of cardiac performance with quantitative radionuclide angiocardiography. *Circulation* 1977; 56:820–829.
23. Schelbert HR, Verba JW, Johnson AD, et al. Nontraumatic determination of left ventricular ejection fraction by radionuclide angiocardiography. *Circulation* 1975;51:902–909.
24. National Electrical Manufacturer's Association. Performance measurements of scintillation cameras. *Standards publication no. NU1-1986*. Washington DC: NEMA; 1986.
25. Wackers FJT, Berger HJ, Johnstone DE, et al. Multiple gated cardiac blood pool imaging for left ventricular ejection fraction: validation of the technique and assessment of variability. *Am J Cardiol* 1979;43:1159–1166.
26. Jengo JA, Oren V, Conant R, et al. Effects of maximal exercise stress on left ventricular function in patients with coronary artery disease using first pass radionuclide angiocardiography. *Circulation* 1979;59:60–65.
27. Wackers FJT, Sinusas A, Saari MA, Mattera JA. Is list mode ECG-gated first pass LVEF accurate using a single crystal gamma camera? Implications for ^{99m}Tc-labeled perfusion imaging agents [Abstract]. *J Nucl Med* 1991;32: 939.
28. Berger HJ, Matthay RA, Loke J, Marshall RC, Gottschalk A, Zaret BL. Assessment of cardiac performance with quantitative radionuclide angiocardiography: right ventricular ejection fraction with reference to findings in chronic obstructive pulmonary disease. *Am J Cardiol* 1978;41:897–905.
29. Rezai K, Weiss R, Stanford W, Preslar J, Marcus M, Kirchner P. Relative accuracy of three scintigraphic methods for determination of right ventricular ejection fraction: a correlative study with ultrafast computed tomography. *J Nucl Med* 1991;32:429–435.
30. Gelfand MJ. First-pass measurement of ejection fraction. In: Gelfand MJ, Thomas SR, eds. *Effective use of computers in nuclear cardiology: practical clinical applications in the imaging laboratory*. New York: McGraw-Hill, Inc.; 1988;206–227.
31. Budinger TF, Rollo FD. Physics and instrumentation in nuclear medicine. *Prog Cardiovasc Dis* 1977;20:19–54.
32. Port S, Gal R, Grenier R, Acharya K, Shen Y, Skrade B. First-pass radionuclide angiography during treadmill exercise: evaluation of patient motion and a method for motion correction [Abstract]. *J Nucl Med* 1989;30: 770.
33. Zaret BL, Wackers FJ, Soufer R. Nuclear cardiology. In: Braunwald E, ed. *Heart disease: a textbook of cardiovascular medicine*, 4th edition. Philadelphia: W. B. Saunders Company; 1992:276–311.
34. Wackers FJ, Giles RW, Hoffer PB, et al. Gold-195m, a new generator-produced short-lived radionuclide for sequential assessment of ventricular performance by first-pass radionuclide ventriculography. *Am J Cardiol* 1982;50:89–94.
35. Mena I, Narahar K, DeJong R, Maublant J. Gold-195m, an ultra short-lived generator-produced radionuclide: clinical application in sequential first-pass ventriculography. *J Nucl Med* 1983;24:139–144.